Atmos. Chem. Phys. Discuss., 11, 29807–29843, 2011
www.atmos-chem-phys-discuss.net/11/29807/2011/
doi:10.5194/acpd-11-29807-2011

Atmospheric Chemistry and Physics Discussions

Satellite constraint for emissions of nitrogen oxides from anthropogenic, lightning and soil sources over East China on a high-resolution grid

J.-T. Lin

Laboratory for Climate and Ocean-Atmosphere Studies, Department of Atmospheric and Oceanic Sciences, School of Physics, Peking University, Beijing 100871, China

Received: 28 September 2011 – Accepted: 25 October 2011 – Published: 7 November 2011

Correspondence to: J.-T. Lin (linjt@pku.edu.cn)

Published by Copernicus Publications on behalf of the European Geosciences Union.

Abstract

Vertical column densities (VCDs) of tropospheric nitrogen dioxide (NO_2) retrieved from space provide valuable information to estimate emissions of nitrogen oxides (NO_x) inversely. Accurate emission attribution to individual sources, important both for understanding the global biogeochemical cycling of nitrogen and for emission control, remains difficult. This study presents a regression-based multi-step inversion approach to estimate emissions of NO_x from anthropogenic, lightning and soil sources individually for 2006 over East China on a 0.25° long × 0.25° lat grid, employing the DOMINO product version 2 retrieved from the Ozone Monitoring Instrument. The nested GEOS-Chem model for East Asia is used to simulate the seasonal variations of different emission sources and impacts on VCDs of NO_2 for the inversion purpose. Sensitivity tests are conducted to evaluate key assumptions embedded in the inversion process. The inverse estimate suggests annual budgets of about 7.1 TgN (±38 %), 0.22 TgN (±46 %), and 0.40 TgN (±48 %) for the a posteriori anthropogenic, lightning and soil emissions, respectively, each about 24 % higher than the respective a priori values. The enhancements in anthropogenic emissions are largest in cities and areas with extensive use of coal, particularly in the north in winter, as evident on the high-resolution grid. Derived soil emissions are consistent with recent bottom-up estimates. They are each less than 6 % of anthropogenic emissions annually, increasing to about 13 % for July. Overall, anthropogenic emissions are found to be the dominant source of NO_x over East China with important implications for nitrogen control.

1 Introduction

Nitrogen oxides ($NO_x \equiv NO + NO_2$) are important constituents in the troposphere affecting the formation of ozone and aerosols with significant consequences on air quality, climate forcing and acid deposition. They are emitted from anthropogenic combustion sources as well as natural sources from lightning, soil and biomass burning.

ACPD
11, 29807–29843, 2011

Understanding the individual contributions of anthropogenic and natural emissions is critical both for evaluating the effects of NO_x on the global environment and for forming appropriate emission control strategies in polluted areas like East China.

Satellite remote sensing provides data for vertical column densities (VCDs) of nitrogen dioxide (NO_2) in the troposphere. The data can be used to estimate emissions of NO_x from the top-down perspective supplementing the bottom-up estimate (Martin et al., 2003; Jaeglé et al., 2005; Müller and Stavrakou, 2005; Richter et al., 2005; Martin et al., 2006; Wang et al., 2007; Zhang et al., 2007; Stavrakou et al., 2008; Zhao and Wang, 2009; Lin et al., 2010a,b; Lin and McElroy, 2010; Lin and McElroy, 2011). Retrieved VCDs, however, include contributions from all sources of NO_x, requiring additional information and assumptions in distinguishing individual sources.

Several inversion studies have attempted to separate anthropogenic from other sources of NO_x, especially soil sources, based on measurements from the Global Ozone Monitoring Experiment (GOME) instrument (Jaeglé et al., 2005; Müller and Stavrakou, 2005; Wang et al., 2007; Stavrakou et al., 2008), the Scanning Imaging Absorption Spectrometer for Atmospheric CHartographY (SCIAMACHY) instrument (Müller and Stavrakou, 2005; Stavrakou et al., 2008), and the Ozone Monitoring Instrument (OMI) (Zhao and Wang, 2009). Jaeglé et al. (2005) and Wang et al. (2007) proposed two different methods to separate anthropogenic, soil and biomass burning emissions month by month with no attempt to constrain lightning emissions. Jaeglé et al. (2005) assumed the a posteriori non-lightning emissions to be solely anthropogenic if the a priori anthropogenic emissions exceed 90 % of the a priori total emissions or if they exceed the a posteriori non-lightning emissions. Otherwise, differences between the a posteriori and a priori emissions were attributed to soil or biomass burning sources. A similar criterion was adopted by Zhao and Wang (2009) to differentiate anthropogenic and soil emissions. Wang et al. (2007) distinguished anthropogenic and soil sources using prescribed values for errors in the a priori anthropogenic emission data. Specifically, if the a posteriori non-lightning non-biomass burning emissions exceed the a priori anthropogenic emissions plus errors (assumed to be 40–

ACPD
11, 29807–29843, 2011

60 %), the differences are attributed to soil sources. Müller and Stavrakou (2005) and Stavrakou et al. (2008) used an adjoint modeling approach for source attribution. Wang et al. (2007) suggested that soil emissions over East China amounted to 0.85 TgN per year for 1997–2000, differing significantly from other inverse estimates (Jaeglé et al., 2005; Müller and Stavrakou, 2005; Stavrakou et al., 2008; Zhao and Wang, 2009; Lyatt Jaeglé, personal communication, 2011; Chun Zhao and Yuhang Wang, personal communication, 2011). Soil emissions derived from the inverse modeling also differ from the bottom-up estimates (Yienger and Levy, 1995; Yan et al., 2003, 2005; Hudman et al., 2011; Steinkamp and Lawrence, 2011); in particular, they are 50–300 % larger than the Yienger and Levy (1995) estimate. According to Jaeglé et al. (2005) and Wang et al. (2007), soil emissions may be as large as 40–50 % of anthropogenic emissions in summer for East Asia in 2000 and for East China in 1997–2000, respectively, with significant implications for the global biogeochemical cycling of nitrogen. The magnitude of lightning emissions is difficult to estimate (Boersma et al., 2005; Schumann and Huntrieser, 2007), especially on the regional scale with significant variations in lightning occurrences from one year to another (Schumann and Huntrieser, 2007). Most inverse estimates did not attempt to constrain lightning emissions (Jaeglé et al., 2005; Wang et al., 2007; Zhao and Wang, 2009; Lin et al., 2010a,b; Lin and McElroy, 2010). The inverse modeling by Stavrakou et al. (2008) suggested lightning emissions to be 50–80 % larger than their a priori values (3 TgN yr^{-1} globally) with the largest difference over the tropics; the study did not specify the magnitude of lightning emissions over China.

This study presents a new method to inversely derive emissions of NO_x for 2006 over East China (101.25° E–126.25° E, 19°–46° N; see Fig. 1) from anthropogenic, lightning and soil sources individually based on satellite retrievals of NO_2 columns and simulations of the global chemical transport model (CTM) GEOS-Chem. Emissions from biomass burning are not constrained since they are unimportant over East China (Lin et al., 2010a). A regression-based multi-step inversion approach is used to derive emissions for all months, exploiting information on the seasonal variations of individual

ACPD
11, 29807–29843, 2011

sources simulated by the CTM. The satellite data are taken from the DOMINO product version 2 (DOMINO-2) retrieved by the Royal Netherlands Meteorological Institute (KNMI) from the Ozone Monitoring Instrument (OMI) (Boersma et al., 2007, 2011). The nested GEOS-Chem model for East Asia (Chen et al., 2009) is used to calculate VCDs of NO_2 in response to various emission sources for the inversion purpose. The top-down emissions are derived at a relatively fine resolution of 0.25° long × 0.25° lat allowing for a more detailed analysis of the spatial distribution of emissions, compared to previous studies (Jaeglé et al., 2005; Müller and Stavrakou, 2005; Wang et al., 2007; Stavrakou et al., 2008; Zhao and Wang, 2009).

The paper is organized as follows. Section 2 presents the satellite product. Section 3 describes the CTM and compares simulated VCDs with retrieved values. Section 4 describes the inversion process in detail and analyzes the resulting top-down emissions for anthropogenic, lightning and soil sources. It also evaluates the effects of key assumptions made during the inversion process. Section 5 presents the a posteriori emissions in comparison with previous inverse and bottom-up estimates. Section 6 concludes the present analysis.

2 VCDs of NO_2 retrieved from OMI

The KNMI DOMINO-2 product offers a level-2 dataset for VCDs of NO_2 derived by three main steps involving the calculation of slant column densities (SCDs), tropospheric SCDs, and tropospheric VCDs (Boersma et al., 2007, 2011). The derivation relies on information on air mass factors (AMFs) to convert the tropospheric SCDs to VCDs. The AMFs are interpolated from a look-up table (LUT), and are subject to errors in the predetermined information for clouds, aerosols, surface albedo, the a priori vertical profile of NO_2, surface pressure, and surface height. The reader is referred to Boersma et al. (2007, 2011) for detailed derivation of the product.

Errors in retrieved VCDs are derived mainly from the calculation of SCDs and its tropospheric portion over cleaner regions, and are mainly from the calculation of AMFs

ACPD
11, 29807–29843, 2011

for polluted regions (Boersma et al., 2007). Compared to version 1, DOMINO-2 incorporates a variety of improvements on the LUT, surface albedo, and the a priori vertical profile of NO_2 (Boersma et al., 2011). It also includes a cross-track stripe correction and a high-resolution dataset for surface height. As a result, systematic biases found in version 1 are reduced significantly in DOMINO-2 (Boersma et al., 2011). The overall error for retrieved VCDs in DOMINO-2 is estimated to be about 30 % (a relative error) plus 0.7×10^{15} molec cm^{-2} (an absolute error), likely with a magnitude larger in winter than in summer (Boersma et al., 2007, 2011; Lin and McElroy, 2010; Lin et al., 2010a; Lin and McElroy, 2011). In this study, the relative error is assumed to vary nonlinearly from 30 % in summer to 50 % in winter (Fig. 2). This information will be employed and evaluated for purposes of emission inversion.

In this study, the daily level-2 data from DOMINO-2 are gridded to 0.25° long × 0.25° lat, which are averaged then to obtain monthly mean VCDs for subsequent emission inversion. The level-2 dataset includes measurements at 60 viewing angles corresponding to 60 ground pixels, and the pixel sizes increase nonlinearly from 13×24 km^2 at nadir to $25 \times \sim 140$ km^2 at the edges of the viewing swath. This study only uses data from the 30 pixels around the swath center (with a cross-track length less than 30 km), allowing for a better analysis of the spatial distribution of VCDs within short distances. Note that the pixel sizes here are much smaller than the GOME (320×40 km^2) and SCIAMACHY (60×30 km^2) instruments used in previous inverse estimates (Jaeglé et al., 2005; Müller and Stavrakou, 2005; Wang et al., 2007; Stavrakou et al., 2008).

3 Simulations of GEOS-Chem

3.1 Descriptions of model simulations

This study uses the nested model of GEOS-Chem (version 08-03-02; http://wiki.seas.harvard.edu/geos-chem/index.php/MainPage) for East Asia run at a horizontal resolution of 0.667° long × 0.5° lat with 47 layers vertically (Chen et al., 2009). The model is

ACPD
11, 29807–29843, 2011

run with the full O_x–NO_x–CO–VOC–HO_x chemistry. The lateral boundary conditions are updated every 3 h using results from associated global simulations at 5° long × 4° lat horizontally. Both global and nested simulations are driven by the assimilated meteorological fields of GEOS-5 taken from the National Aeronautics and Space Administration (NASA) Global Modeling and Assimilation Office (GMAO).

Annual anthropogenic emissions of NO_x, carbon monoxide (CO) and non-methane volatile organic compounds (VOC) are taken from the INTEX-B dataset for 2006 provided by Zhang et al. (2009), including sources from power plants, industry, transportation and the residential sector. Emissions from the residential sector are further assumed to vary month to month accounting for heating related emissions that depend on ambient air temperature (Streets et al., 2003). They, however, contribute only to 6 % of anthropogenic sources of NO_x on the annual basis (Zhang et al., 2009). Emissions from power plants, industry and transportation are held constant across the seasons since the seasonality is relatively small and is not included in the INTEX-B dataset. The impact of such simplification is found to be small (see Sect. 5). The diurnal variations of individual sources follow Lin et al. (2010a) and Lin and McElroy (2010, 2011).

Natural sources of NO_x include lightning, soil and biomass burning. In GEOS-Chem, emissions from lightning follow the formulation of Price et al. (1997) with specified vertical distributions (Ott et al., 2010) and adjustments for horizontal distribution (Murray et al., 2011; Sauvage et al., 2007). Soil emissions are based on the Yienger and Levy (1995) scheme with the canopy reduction factors described by Wang et al. (1998). They include sources due to microbiological processes producing NO_x naturally as well as those associated with use of chemical fertilizers and manure. As normally assumed, fertilizer associated soil emissions are considered to be part of natural sources in this study for comparison with anthropogenic emissions relating to combustion. Emissions from biomass burning are taken from the monthly dataset of GFED2 (van der Werf et al., 2006); their magnitudes are negligible for NO_x over China (Lin et al., 2010a).

A total of five 1-yr simulations for 2006 were conducted to quantify VCDs of NO_2 from anthropogenic, lightning, soil and biomass burning sources, as shown in Table 1. For

ACPD
11, 29807–29843, 2011

consistency with satellite retrievals, model VCDs are obtained by regridding modeled NO_2 at each vertical layer to 0.25° long × 0.25° lat and applied with the averaging kernel from DOMINO-2.

Potential sources of model errors include emissions of NO_x, emissions of other pollutants affecting the chemistry of NO_x, the chemical mechanism for NO_x, the scheme for mixing in the boundary layer, and the meteorological fields. The total model error from factors other than emissions of NO_x is estimated to be about 30–40 % (Martin et al., 2003; Wang et al., 2007; Lin and McElroy, 2011); in this study, the value of 40 % is taken for the inversion purpose.

3.2 Comparison between simulated and retrieved VCDs of NO_2

Figure 3 compares retrieved VCDs with simulated values (from all sources; Case 1 in Table 1) for January, April, July, October and annual average for 2006. Retrieved VCDs are large in regions with more advanced economic and industrial development and/or dense population, including the coastal and neighbor provinces from Beijing to Shanghai, the Pearl River Delta and the Sichuan Basin. Spike values are evident over major cities. In addition, retrieved VCDs vary across the months significantly, reaching maximum values in January and minimum values in July.

GEOS-Chem captures fairly well the spatial distributions of retrieved VCDs in different seasons (Fig. 3). The R^2 for spatial correlation between modeled and retrieved VCDs reaches 0.64 for January and 0.53 for July (Table 2). The smaller correlation in July is in part because the native horizontal resolution of the CTM (0.667° long × 0.5° lat) is not fine enough to capture the large spatial variation of VCDs within short distances resulting from the short lifetime of NO_x (Martin et al., 2003; Lin et al., 2010a). Spatial smoothing of 3 gridboxes by 3 gridboxes (i.e., 0.75° long by 0.75° lat) results in a significant enhancement of model-retrieval correlation in July with the R^2 increasing to 0.67. The improvement of R^2 due to the smoothing is moderate in January, compared to July, since the lifetime of NO_x is longer and the spatial variability of VCDs within short distances is smaller and better simulated by GEOS-Chem.

ACPD
11, 29807–29843, 2011

GEOS-Chem underestimates the magnitude of retrieved VCDs particularly over polluted regions in wintertime (Fig. 3). The range of simulated VCDs is also narrower than the retrieved range: spatially, the modeled maximum VCD is lower than the retrieved maximum with the minimum being higher (Table 2). Averaged over East China, model VCDs are about 20 % lower than retrieved values in July and about 36 % lower in January (Table 2).

4 Inversion of anthropogenic, lightning and soil emissions

4.1 Method

As shown in Fig. 4, the a priori anthropogenic emissions of NO_x are relatively constant across the seasons, while lightning and soil sources reach maximum values in summer and are not important in winter. In addition, the lifetime of NO_x is shortest in summer and longest in winter as a result of varying photochemical activity (Martin et al., 2003; Lin et al., 2010a; Lin and McElroy, 2010). This results in minimum values in summer for VCDs of NO_2 of anthropogenic origin and maximum values for NO_2 from natural sources, as simulated by GEOS-Chem (Fig. 5). Averaged over East China, natural sources contribute to about 30 % of the total abundance of NO_2 in July and August, in contrast to their negligible contributions in winter months. This characteristic is exploited here to estimate anthropogenic and natural emissions separately.

The inversion here involves a multi-step process based on a weighted multivariate linear regression analysis facilitated by several supplementary procedures. The regression is described in Sect. 4.1.1. The complete inversion process is described in Sect. 4.1.2 together with the supplementary procedures.

4.1.1 A weighted multivariate linear regression analysis

Neglecting horizontal transport and assuming a linear relationship between the total VCD of NO_2 and VCDs from individual sources, the retrieved VCD of NO_2 for a given

ACPD
11, 29807–29843, 2011

gridbox (of 0.25° long × 0.25° lat) in a given month can be approximated as the sum of modeled VCDs from individual emission sources, multiplied by certain scaling factors, and a random error term:

$$\Omega_r = k_a\Omega_{m,a} + k_l\Omega_{m,l} + k_s\Omega_{m,s} + k_b\Omega_{m,b} + \varepsilon \quad (1)$$

where $\Omega_m = \Omega_{m,a} + \Omega_{m,l} + \Omega_{m,s} + \Omega_{m,b}$.

Here Ω_r denotes retrieved VCD of NO_2, and Ω_m denotes modeled VCD. The error term ε is assumed to follow a normal distribution with zero mean and standard deviation (σ) equal to the sum in quadrature of errors from Ω_r and Ω_m. The subscripts "a", "l", "s", and "b" indicate anthropogenic, lightning, soil, and biomass burning sources of NO_x, respectively. The coefficient k denotes the scaling factors for individual sources to be determined by the inversion process. The VCD that can be predicted from the inversion process is:

$$\Omega_p = k_a\Omega_{m,a} + k_l\Omega_{m,l} + k_s\Omega_{m,s} + k_b\Omega_{m,b} \quad (2)$$

and the top-down emission is calculated as the sum of the a priori emissions from individual sources multiplied by corresponding scaling factors:

$$E_t = k_aE_{a,a} + k_lE_{a,l} + k_sE_{a,s} + k_bE_{a,b} \quad (3)$$

Here a linear relationship is assumed for each source between emissions of NO_x and VCDs of NO_2. Ω_r, Ω_m and σ are known variables, and they vary from one month to the next. By minimizing the sum of $[(\Omega_r - \Omega_p)/\sigma]^2$ in all months, Eqs. (1) and (2) serve as a weighted multivariate linear regression model to determine the scaling factors. Here the scaling factors are assumed implicitly to be season independent.

Over China, the contribution of biomass burning is very small for NO_x, thus we do not attempt to constrain the associated emissions: k_b is set as unity. Emissions from lightning and soil vary with seasons with similar patterns (Fig. 4), thus it is difficult to distinguish their contributions accurately based on the regression approach. Therefore

ACPD
11, 29807–29843, 2011

the scaling factors for the two sources are assumed to be the same in conducting the regression analysis. Under these assumptions, Eqs. (1)–(3) reduce to:

$$\Omega_r = k_a \Omega_{m,a} + k_l(\Omega_{m,l} + \Omega_{m,s}) + \Omega_{m,b} + \varepsilon \quad (4)$$

$$\Omega_p = k_a \Omega_{m,a} + k_l(\Omega_{m,l} + \Omega_{m,s}) + \Omega_{m,b} \quad (5)$$

$$E_t = k_a E_{a,a} + k_l(E_{a,l} + E_{a,s}) + E_{a,b} \quad (6)$$

The regression model here provides a basic statistical tool to calculate k_a and k_l. It is necessary to determine the ranges of k_a and k_l to facilitate the regression analysis; without such constraints the derived scaling factors may be unrealistic for certain gridboxes (too high, too low or even negative). k_a is set to range from 0.33 to 3 reflecting that uncertainties in anthropogenic emissions are normally moderate for individual gridboxes. Uncertainties in natural emissions are expected to be larger than those in anthropogenic emissions, therefore k_l is set to vary between 0.2 and 5.

4.1.2 A multi-step inversion process beyond the regression analysis

To better estimate k_a and k_l, the gridboxes are allocated to different groups for ancillary procedures supplementing the regression analysis. The ratio Ω_r/Ω_m differs between winter and summer due in part to the season-dependent contribution of natural sources to the abundance of NO_2 and the relative magnitudes of errors in the a priori natural versus anthropogenic emissions. Thus the seasonally varying ratio is used to categorize the gridboxes, followed by a multi-step procedure to calculate k_a and k_l for all gridboxes (Fig. 6).

Gridboxes are assigned to group 1 if the ratio Ω_r/Ω_m for a selected winter month is smaller than the ratio for a selected summer month; otherwise they are assigned to group 2. For gridboxes in group 1, the regression analysis is performed to calculate k_a and k_l (step 1 in Fig. 6). Results are discarded if the regression is not statistically significant at a significance level of 0.1 under the Chi-square test. Spatial interpolation

ACPD
11, 29807–29843, 2011

(step 2 in Fig. 6) is then conducted iteratively to derive k_l for all gridboxes: for a gridbox with undetermined k_l, the value of k_l is calculated as the geometric mean of values in the surrounding 24 gridboxes derived previously. For gridboxes in group 2, the regression analysis usually results in unrealistically low values for k_l and thus is used to estimate k_a only (step 3 in Fig. 6); the value of k_l has been determined at previous steps. Again, the result is discarded if the regression is not statistically significant.

The regression approach may not be appropriate for certain gridboxes with unrealistically large Ω_r/Ω_m ratios in the winter month. This is because the scaling factor k_a likely has a significant seasonal dependence as a result of the seasonality in anthropogenic emissions not fully accounted for in the a priori dataset. These gridboxes are therefore reassigned to a third group, where a k_a is derived for each month as the ratio $[\Omega_r - k_l(\Omega_{m,l} + \Omega_{m,s}) - \Omega_{m,b}]/\Omega_{m,a}$ (step 4 in Fig. 6). Tentatively, a gridbox is allocated to group 3 if the ratio Ω_r/Ω_m exceeds 3, or if the ratio exceeds 2 with Ω_r being higher than 6×10^{15} molec cm^{-2}, in the winter month.

As a final step, spatial interpolation is conducted to obtain k_a for gridboxes of groups 1 and 2 where the regression is not statistically significant (step 5 in Fig. 6).

In group allocation and subsequent inversion process, each of three winter months (December, January and February) is paired with each of two summer months (July and August) to generate a suite of six cases for winter-summer contrast. (June is not selected since the contribution of natural sources to the total abundance of NO_2 is not as significant as that in July or August.) Results from the six cases are combined to obtain final values of k_a and k_l. Specifically, results at a given step available from any or all of the six cases are geometrically averaged to obtain final values of k_a and k_l, if and only if they have not been derived at earlier steps.

4.2 Scaling factors estimated for anthropogenic, lightning and soil sources

The scaling factors are determined at step 1 for most gridboxes (Figs. 7 and 8). At this step, the values of k_a are around unity in most areas, are consistently larger than 1 over the southwestern provinces, and vary between 1 and 2 in many of the remaining

ACPD
11, 29807–29843, 2011

areas with stripe patterns (Fig. 7). By comparison, k_l varies more significantly from one location to the next (Fig. 8). It reaches maximum values in southern Hebei Province and along the northern coasts of the Bohai Sea, and also has spike values in parts of the western provinces.

The special treatment at step 4 is taken mainly for gridboxes in and around Shanxi Province and in parts of Ningxia and Inner-Mongolia (Fig. 7). These places are main areas in China for coal mining and coal-fired electricity generation. The large values of k_a in these places, particularly in winter, suggest that the a priori dataset from INTEX-B likely underestimates anthropogenic sources related to use of coal, consistent with the findings of Wang et al. (2010).

The final values of k_a and k_l are determined at step 5 (see Fig. 7 for January) and step 2 (Fig. 8), respectively, for all gridboxes. They are used to calculate the top-down emissions for respective sources.

4.3 VCDs of NO_2 predicted from the inversion process

Compared to simulation results, predicted VCDs are much closer to retrieved values (Fig. 3). The spatial correlation between predicted and retrieved VCDs is much higher than the correlation between simulated and retrieved VCDs, with the R^2 increasing from 64 % to 83 % in January and from 53 % to 86 % in July (Table 2). Averaged over East China, predicted VCDs are within 15 % of retrieved values across the seasons.

4.4 Top-down emissions

Figure 9 compares the top-down emissions of NO_x for anthropogenic, lightning and soil sources with respective a priori emissions for July. Both top-down and a priori datasets suggest significant anthropogenic sources over the coastal provinces from Shanghai to Beijing and over the Pearl River Delta, resulting in large concentrations of NO_2 (Fig. 10). The top-down anthropogenic emissions are much higher than the a priori emissions in cities and at locations with extensive use of coal, especially in the northern provinces.

ACPD
11, 29807–29843, 2011

In July, emissions from lightning are large in the north as a result of strong convection events associated with the summer monsoon (Fig. 9). Soil emissions are greatest in major agricultural areas in Hebei, Henan, Shandong and parts of neighbor provinces (Fig. 9). The top-down estimates for lightning and soil emissions are much larger than the a priori values at many places of the respective source regions.

The contribution of anthropogenic sources to the total emissions of NO_x in July is generally consistent between the a priori and top-down datasets (Fig. 9). The anthropogenic contribution exceeds 80 % over large areas of East China, but is lower than 60 % over most of the northwest and Inner-Mongolia. It differs from the anthropogenic contribution to the VCD of NO_2 (Fig. 10). This is in part because lightning emissions occur at higher altitudes with longer lifetime of NO_x than near the ground, compensated to some extent by a reduced fraction of NO_2 in NO_x. Another factor is the use of averaging kernel in deriving model VCDs. The averaging kernel is larger for NO_2 of lightning origin at higher altitudes and lower for NO_2 derived from the ground. Thus the contribution is enhanced for a given amount of lightning emissions to the total abundance of NO_2, compared to the same amount of emissions from the ground. The effect is evident particularly over the southwest. In addition, data for simulated VCDs are sampled at the time of day of satellite overpass from days with valid retrieval data; while data for monthly emissions are averaged over all time of day in all days of the month. The different sampling methods and the day-to-day and diurnal variations in natural emissions may introduce some differences between anthropogenic contributions to total emissions and to total VCDs. Another possible cause is the neglect of horizontal transport likely introducing uncertainties in source attribution for relatively clean regions downwind of polluted areas, e.g., at many places of Inner-Mongolia.

Table 3 compares the a priori and top-down emission budgets over East China for individual sources. Annually, the inversion results in budgets of 8.016 TgN, 0.228 TgN and 0.424 TgN for anthropogenic, lightning and soil emissions, respectively. These values are about 39 %, 31 % and 31 % larger than the corresponding a priori estimates. The top-down datasets also suggest that both lightning and soil emissions are less

ACPD
11, 29807–29843, 2011

than 6 % of anthropogenic emissions. For July, the top-down budgets for lightning and soil emissions are 0.0623 TgN and 0.0810 TgN, respectively, about 10 % and 13 % of anthropogenic emissions estimated at 0.646 TgN.

4.5 Improved GEOS-Chem simulations using the top-down emissions

The inversion approach presented here assumes a linear relationship for a given gridbox between the total VCD of NO_2 and VCDs from individual sources and between emissions of NO_x and VCDs of NO_2. It also neglects horizontal transport, which may introduce uncertainties in deriving emissions for individual gridboxes. To evaluate the reliability of the inversion results, sensitivity simulations of GEOS-Chem were conducted for January and July 2006 by using the top-down emissions to drive the CTM. As shown in Fig. 3, VCDs resulting from the sensitivity simulations reproduce the spatial distribution of retrieved VCDs in both months. The R^2 for spatial correlation reaches a high level of 81 % for January and 66 % for July (Table 2). The smaller correlation in July is due to the short lifetime of NO_x such that the CTM (at 0.667° long × 0.5° lat) is not able to simulate the large spatial variation of NO_2 within short distances, as discussed in Sect. 3.2. After (3 gridboxes by 3 gridboxes) horizontal smoothing, the R^2 increases to 88 % for January and 81 % for July (Table 2). Averaged over East China, the magnitude of model VCD is about 10 % higher than the predicted value in January and about 5 % lower in July (Table 2), indicating a slight nonlinear relationship between emissions and VCDs.

4.6 Sensitivity of emission inversion to embedded assumptions

This section evaluates the effects on the top-down emissions of several important assumptions taken during the inversion process. The results are summarized in Table 3.

The regression here relies on assumptions on the seasonal variations of individual emission sources. Anthropogenic emissions from power plants, industry and transportation differ slightly among seasons (Zhang et al., 2009), but are assumed here to be season independent for simulations of GEOS-Chem. The assumption was

ACPD
11, 29807–29843, 2011

evaluated by a sensitivity analysis taking into account the seasonality estimated by Zhang et al. (2009). Specifically, modeled anthropogenic VCDs ($\Omega_{m,a}$) for individual months were scaled prior to the inversion by the seasonality of total anthropogenic emissions derived from Table 9 of Zhang et al. (2009). This resulted in increases by less than 15 % in top-down lightning/soil emissions (Case 2 in Table 3). The effect is smaller than 5 % for top-down anthropogenic emissions.

The regression accounts for the seasonal dependence of retrieval errors (Fig. 2). A sensitivity test assuming a time invariant relative error of 30 % resulted in decreases by less than 5 % in top-down lightning/soil emissions (Case 3 in Table 3). Therefore the inversion approach is not sensitive to the seasonality of retrieval errors assumed here.

Another test was taken to evaluate the effect of errors in the Yienger and Levy (1995) soil emissions used as our a priori estimate. Specifically, the updated emission data by Hudman et al. (2011) were used to adjust modeled VCDs from soil sources ($\Omega_{m,s}$) prior to the inversion, by scaling the VCDs for individual gridboxes with the ratios of Hudman et al. over Yienger and Levy soil emissions. As a result, the annual top-down lightning emissions were reduced by 11 % and soil emissions enhanced by 19 % (Case 4 in Table 3).

The inversion approach allocates individual gridboxes to three groups prior to the regression. The effect of group allocation was evaluated by two tests, one by re-allocating gridboxes in group 2 to group 1 and the other by re-allocating gridboxes in both group 2 and group 3 to group 1. The tests suggested that the effect of group allocation is less than 15 % for top-down lightning/soil emission budgets for East China (Cases 5 and 6 in Table 3) with much larger impacts for individual locations (not shown).

This study only includes 30 out of the 60 pixels from each OMI scan with smaller sizes in order to better analyze the spatial distribution of nitrogen within short distances. The top-down emission budgets for individual sources are similar to results from a sensitivity calculation employing OMI data from all pixels (Case 7 in Table 3); the differences are larger for individual locations (not shown).

ACPD
11, 29807–29843, 2011

Jaeglé et al. (2005), Wang et al. (2007) and Zhao and Wang (2009) assumed lightning emissions to be simulated well by the CTM with no attempt to constrain them inversely. Under the same assumption, a sensitivity analysis was conducted by keeping lightning emissions unchanged during the inversion process here. This resulted in a 52 % increase in the top-down soil emission budget on the annual basis and a 41 % increase for July (Case 8 in Table 3).

If soil emissions are held unchanged during the inversion process, the top-down lightning emissions will be increased by less than 6 % (Case 9 in Table 3).

Errors in the top-down emission budgets attributable to assumptions in the inversion process are calculated as the standard deviation of results from all inversions performed (Cases 1–9 in Table 3): ∼2 % for anthropogenic emissions, ∼ 11 % for lightning emissions, and ∼20 % for soil emissions.

4.7 Total errors in the top-down emissions

The inverse estimate here is subject to errors in retrievals, errors in model simulations, and errors in the inversion procedures as estimated from the sensitivity analyses. The total error in the top-down emissions is taken to be the sum in quadrature of the three errors, amounting to about 50 %, 51 % and 55 % for anthropogenic, lightning and soil sources, respectively.

5 A posteriori emissions

The a posteriori emissions are estimated as the average of the a priori and top-down emissions weighted by the inverse-square of their respective errors (Martin et al., 2003). Errors in the a priori emissions are taken to be 60 % for anthropogenic sources (Wang et al., 2007; Zhao and Wang, 2009) increasing to 100 % for lightning/soil sources accounting for the large range of current estimates (Boersma et al., 2005; Jaeglé et al., 2005; Schumann and Huntrieser, 2007; Wang et al., 2007; Zhao and

ACPD
11, 29807–29843, 2011

Wang, 2009; Lin et al., 2010a). As a result, the a posteriori emissions for 2006 over East China amount to 7.091 TgN (±38 %) for anthropogenic sources, to 0.217 TgN (±46 %) for lightning sources, and to 0.401 TgN (±48 %) for soil sources (Table 3). For July, the a posteriori budgets are 0.578 TgN (±38 %), 0.0599 TgN (±46 %), and 0.0769 TgN (±47 %), respectively. The temporal and spatial distributions of the a posteriori emissions are presented in Figs. 4 and 9 for comparison with the a priori and top-down emissions.

5.1 Comparison with previous estimates

That anthropogenic emissions inferred from space are larger than bottom-up inventories for China is consistent with results from many previous studies (Jaeglé et al., 2005; Wang et al., 2007; Zhang et al., 2007; Lin and McElroy, 2011). Our a posteriori budget for anthropogenic emissions over East China is similar to the value of 0.565 TgN for July 2007 estimated by Zhao and Wang (2009). This study further pinpoints, at a higher resolution, cities and areas with extensive use of coal to be the main regions where bottom-up inventories likely underestimate anthropogenic emissions. Evaluation of lightning emissions is more difficult due to the large uncertainty in current research (Boersma et al., 2005; Schumann and Huntrieser, 2007) and the significant interannual variability of lightning occurrences on the regional scale (Schumann and Huntrieser, 2007). Our a posteriori emissions are within the range of previous estimates (Boersma et al., 2005; Schumann and Huntrieser, 2007; Stavrakou et al., 2008).

Soil emissions of NO_x over China are of great interest concerning the extensive use of fertilizers. A detailed analysis is conducted as follows for our a posteriori estimate of soil emissions.

5.1.1 Comparison with previous satellite-derived soil emission estimates

Wang et al. (2007) suggested that soil emissions are about 0.85 TgN per year for 1997–2000 over East China, amounting to 23 % of anthropogenic emissions on the annual

ACPD
11, 29807–29843, 2011

basis and to as much as 43 % for summer months. In better agreement with our estimates for East China, Jaelgé et al. (2005) found an annual budget of ∼ 0.40 TgN for 2000, and Zhao and Wang (2009) suggested soil emissions to be about 0.0883 TgN for July 2007 (Lyatt Jaeglé, personal communication, 2011; Chun Zhao and Yuhang Wang, personal communication, 2011). The differences are derived mainly from satellite products and methods to separate anthropogenic and natural sources of NO_x employed in individual studies.

5.1.2 Comparison with recent bottom-up estimates for soil emissions

Two new bottom-up estimates have been conducted for soil emissions by Steinkamp and Lawrence (2011) and Hudman et al. (2011), improving upon the work of Yienger and Levy (1995) used as our a priori emissions. The new bottom-up estimates employ information from more recent and complete field measurements to calculate emission factors based on temperature, soil moisture, precipitation and other parameters. They include updated information on the use of fertilizers. Hudman et al. (2011) also combine satellite measurements for growing seasons of vegetation.

Our a posteriori soil emissions at 0.401 TgN (±48 %) annually is consistent with the value of 0.504 TgN estimated by Hudman et al. (2011). They are also within the range of 0.18–0.97 TgN suggested by Steinkamp and Lawrence (2011) (see their Table 7).

6 Conclusions

A regression-based multi-step inversion approach is proposed to estimate emissions of NO_x from anthropogenic, lightning and soil sources for 2006 over East China on a 0.25° long × 0.25° lat grid. It exploits information on VCDs of tropospheric NO_2 retrieved from the OMI instrument by KNMI (the DOMINO product version 2). The nested GEOS-Chem model for East Asia is used to interpret the impacts of individual sources on VCDs of NO_2 to facilitate the inversion analysis.

ACPD
11, 29807–29843, 2011

The inversion starts by allocating the gridboxes to three groups based on analyses of the ratio of retrieved over modeled VCDs in winter and summer. A multivariate regression analysis is used then to derive emissions from individual sources for all months, taking advantage of the seasonal patterns of different sources determined by the CTM. Ancillary procedures are taken to supplement the regression analysis for gridboxes in different groups. Assumptions made during the inversion process contribute to errors in the top-down emission budgets for East China by ∼2 % for anthropogenic sources, ∼11 % for lightning sources and ∼20 % for soil sources. Sensitivity simulations of GEOS-Chem driven by the top-down emission data reproduce the spatial distribution of VCDs retrieved from OMI, with the R^2 for spatial correlation reaching 0.88 for January and 0.81 for July after (3 gridboxes by 3 gridboxes) horizontal smoothing.

The inversion results in an annual budget of 7.091 TgN (±38 %) for the a posteriori anthropogenic emissions of NO_x over East China, about 23 % larger than the INTEX-B dataset (Zhang et al., 2009) used as our a priori emissions. On the 0.25° long × 0.25° lat grid, it is evident that the excess is greater over cities and areas with extensive use of coal, particularly in the north in winter.

The a posteriori budgets are 0.217 TgN (±46 %) and 0.401 TgN (±48 %) for lightning and soil emissions, respectively, for 2006 over East China. Both values are about 24 % higher than the respective a priori estimates, but are less than 6 % of the a posteriori anthropogenic emissions. Even for July, the a posteriori lightning and soil emissions are only about 10 % and 13 % of anthropogenic emissions, respectively. Our results for soil emissions are consistent with recent bottom-up estimates by Steinkamp and Lawrence (2011) and Hudman et al. (2011) and previous inverse estimates by Jaeglé et al. (2005), Stavrakou et al. (2008) and Zhao and Wang (2009). They are however about half of the inverse estimate by Wang et al. (2007) who suggested soil emissions to be more than 40 % of anthropogenic emissions in summer of 1997–2000.

In concluding, anthropogenic emissions are found to be the dominant source of NO_x over East China for 2006, even in summer when natural sources reach maximum values. The contribution of anthropogenic emissions most likely has increased in more

ACPD
11, 29807–29843, 2011

recent years due to their rapid growth (Lin and McElroy, 2011). In the coming future, the anthropogenic contribution may continue to increase along with the rapid economic and industrial development, if emission control is not taken successfully. The importance of nitrogen control has been recognized by the Chinese government, resulting in control strategies targeting the power sector. However, the successfulness of nitrogen control also depends on changes in emissions from other sectors, particularly the industrial sector for which the current inventories may be subject to much larger uncertainties than for the power sector (Zhao et al., 2011). Further research is required to evaluate the effectiveness of nitrogen control and resulting impacts on the contributions of anthropogenic versus natural sources to atmospheric nitrogen burdens.

Acknowledgements. This research is supported by the National Natural Science Foundation of China, grant 41005078 and 41175127. We acknowledge the free use of tropospheric NO_2 column data from www.temis.nl.

References

Boersma, K. F., Eskes, H. J., Meijer, E. W., and Kelder, H. M.: Estimates of lightning NO_x production from GOME satellite observations, Atmos. Chem. Phys., 5, 2311–2331, doi:10.5194/acp-5-2311-2005, 2005.

Boersma, K. F., Eskes, H. J., Veefkind, J. P., Brinksma, E. J., van der A, R. J., Sneep, M., van den Oord, G. H. J., Levelt, P. F., Stammes, P., Gleason, J. F., and Bucsela, E. J.: Near-real time retrieval of tropospheric NO_2 from OMI, Atmos. Chem. Phys., 7, 2103–2118, doi:10.5194/acp-7-2103-2007, 2007.

Boersma, K. F., Eskes, H. J., Dirksen, R. J., van der A, R. J., Veefkind, J. P., Stammes, P., Huijnen, V., Kleipool, Q. L., Sneep, M., Claas, J., Leitão, J., Richter, A., Zhou, Y., and Brunner, D.: An improved tropospheric NO_2 column retrieval algorithm for the Ozone Monitoring Instrument, Atmos. Meas. Tech., 4, 1905–1928, doi:10.5194/amt-4-1905-2011, 2011.

Chen, D., Wang, Y., McElroy, M. B., He, K., Yantosca, R. M., and Le Sager, P.: Regional CO pollution and export in China simulated by the high-resolution nested-grid GEOS-Chem model, Atmos. Chem. Phys., 9, 3825–3839, doi:10.5194/acp-9-3825-2009, 2009.

ACPD

11, 29807–29843, 2011

Hudman, R. C., Moore, N., Martin, R., Russell, A. R., Valin, L. C., and Cohen, R. C.: A mechanistic model of global soil nitric oxide emissions: implementation and space based-constraints on N-pulsing, in preparation, 2011.

Jaeglé, L., Steinberger, L., Martin, R. V., and Chance, K.: Global partitioning of NO_x sources using satellite observations: relative roles of fossil fuel combustion, biomass burning and soil emissions, Faraday Discussions, 130, 407–423, doi:10.1039/b502128f, 2005.

Lin, J.-T. and McElroy, M. B.: Impacts of boundary layer mixing on pollutant vertical profiles in the lower troposphere: implications to satellite remote sensing, Atmos. Environ., 44, 1726–1739, doi:10.1016/j.atmosenv.2010.02.009, 2010.

Lin, J.-T. and McElroy, M. B.: Detection from space of a reduction in anthropogenic emissions of nitrogen oxides during the Chinese economic downturn, Atmos. Chem. Phys., 11, 8171–8188, doi:10.5194/acp-11-8171-2011, 2011.

Lin, J.-T., McElroy, M. B., and Boersma, K. F.: Constraint of anthropogenic NO_x emissions in China from different sectors: a new methodology using multiple satellite retrievals, Atmos. Chem. Phys., 10, 63–78, doi:10.5194/acp-10-63-2010, 2010a.

Lin, J.-T., Nielsen, C. P., Zhao, Y., Lei, Y., Liu, Y., and McElroy, M. B.: Recent changes in particulate air pollution over China observed from space and the ground: effectiveness of emission control, Environ. Sci. Technol., 44, 7771–7776, doi:10.1021/es101094t, 2010b.

Martin, R. V., Jacob, D. J., Chance, K., Kurosu, T. P., Palmer, P. I., and Evans, M. J.: Global inventory of nitrogen oxide emissions constrained by space-based observations of NO_2 columns, J. Geophys. Res., 108, 4537, doi:10.1029/2003JD003453, 2003.

Martin, R. V., Sioris, C. E., Chance, K., Ryerson, T. B., Bertram, T. H., Wooldridge, P. J., Cohen, R. C., Neuman, J. A., Swanson, A., and Flocke, F. M.: Evaluation of space-based constraints on global nitrogen oxide emissions with regional aircraft measurements over and downwind of eastern North America, J. Geophys. Res., 111, D15308, doi:10.1029/2005JD006680, 2006.

Müller, J.-F. and Stavrakou, T.: Inversion of CO and NO_x emissions using the adjoint of the IMAGES model, Atmos. Chem. Phys., 5, 1157–1186, doi:10.5194/acp-5-1157-2005, 2005.

Murray, L. T., Logan, J. A., Jacob, D. J., and Hudman, R. C.: Spatial and interannual variability in lightning constrained by LIS/OTD satellite data for 1998–2006: implications for tropospheric ozone and OH, J. Geophys. Res, submitted, 2011.

Ott, L. E., Pickering, K. E., Stenchikov, G. L., Allen, D. J., DeCaria, A. J., Ridley, B., Lin, R.-F., Lang, S., and Tao, W.-K.: Production of lightning $NO_{(x)}$ and its vertical distribution calculated

ACPD

11, 29807–29843, 2011

from three-dimensional cloud-scale chemical transport model simulations, J. Geophys. Res.-Atmos., 115, D04301, doi:10.1029/2009jd011880, 2010.
Price, C., Penner, J., and Prather, M.: NO_x from lightning, 1, Global distribution based on lightning physics, J. Geophys. Res., 102, 5929–5941, 1997.
Richter, A., Burrows, J. P., Nüß, H., Granier, C., and Niemeier, U.: Increase in tropospheric nitrogen dioxide over China observed from space, Nature, 437, 129–132, doi:10.1038/nature04092, 2005.
Sauvage, B., Martin, R. V., van Donkelaar, A., Liu, X., Chance, K., Jaeglé, L., Palmer, P. I., Wu, S., and Fu, T.-M.: Remote sensed and in situ constraints on processes affecting tropical tropospheric ozone, Atmos. Chem. Phys., 7, 815–838, doi:10.5194/acp-7-815-2007, 2007.
Schumann, U. and Huntrieser, H.: The global lightning-induced nitrogen oxides source, Atmos. Chem. Phys., 7, 3823–3907, doi:10.5194/acp-7-3823-2007, 2007.
Stavrakou, T., Müller, J. F., Boersma, K. F., De Smedt, I., and van der A, R. J.: Assessing the distribution and growth rates of NO_x emission sources by inverting a 10-year record of NO_2 satellite columns, Geophys. Res. Lett., 35, L10801, doi:10.1029/2008gl033521, 2008.
Steinkamp, J. and Lawrence, M. G.: Improvement and evaluation of simulated global biogenic soil NO emissions in an AC-GCM, Atmos. Chem. Phys., 11, 6063–6082, doi:10.5194/acp-11-6063-2011, 2011.
Streets, D. G., Bond, T. C., Carmichael, G. R., Fernandes, S. D., Fu, Q., He, D., Klimont, Z., Nelson, S. M., Tsai, N. Y., Wang, M. Q., Woo, J. H., and Yarber, K. F.: An inventory of gaseous and primary aerosol emissions in Asia in the year 2000, J. Geophys. Res.-Atmos., 108, 8809, doi:10.1029/2002jd003093, 2003.
Wang, S. W., Streets, D. G., Zhang, Q. A., He, K. B., Chen, D., Kang, S. C., Lu, Z. F., and Wang, Y. X.: Satellite detection and model verification of $NO_{(x)}$ emissions from power plants in Northern China, Environ. Res. Lett., 5, 044007, doi:10.1088/1748-9326/5/4/044007, 2010.
Wang, Y., Jacob, D. J., and Logan, J. A.: Global simulation of tropospheric O_3-NO_x-hydrocarbon chemistry, 1. Model formulation, J. Geophys. Res., 103(D9), 10713–10726, 1998.
Wang, Y., McElroy, M. B., Martin, R. V., Streets, D. G., Zhang, Q., and Fu, T.-M.: Seasonal variability of NO_x emissions over East China constrained by satellite observations: Implications for combustion and microbial sources, J. Geophys. Res., 112, D06301, doi:10.1029/2006JD007538, 2007.
van der Werf, G. R., Randerson, J. T., Giglio, L., Collatz, G. J., Kasibhatla, P. S., and Arel-

ACPD
11, 29807–29843, 2011

lano Jr., A. F.: Interannual variability in global biomass burning emissions from 1997 to 2004, Atmos. Chem. Phys., 6, 3423–3441, doi:10.5194/acp-6-3423-2006, 2006.

Yan, X. Y., Akimoto, H., and Ohara, T.: Estimation of nitrous oxide, nitric oxide and ammonia emissions from croplands in East, Southeast and South Asia, Glob. Change Biol., 9, 1080–1096, doi:10.1046/j.1365-2486.2003.00649.x, 2003.

Yan, X. Y., Ohara, T., and Akimoto, I.: Statistical modeling of global soil $NO_{(x)}$ emissions, Global Biogeochem. Cy., 19, Gb3019, doi:10.1029/2004gb002276, 2005.

Yienger, J. J. and Levy, H.: Empirical model of global soil-biogenic NO_x emissions, J. Geophys. Res., 100, 11447–11464, 1995.

Zhang, Q., Streets, D. G., He, K., Wang, Y., Richter, A., Burrows, J. P., Uno, I., Jang, C. J., Chen, D., Yao, Z., and Lei, Y.: NO_x emission trends for China, 1995–2004: the view from the ground and the view from space, J. Geophys. Res., 112, D22306, doi:10.1029/2007JD008684, 2007.

Zhang, Q., Streets, D. G., Carmichael, G. R., He, K. B., Huo, H., Kannari, A., Klimont, Z., Park, I. S., Reddy, S., Fu, J. S., Chen, D., Duan, L., Lei, Y., Wang, L. T., and Yao, Z. L.: Asian emissions in 2006 for the NASA INTEX-B mission, Atmos. Chem. Phys., 9, 5131–5153, doi:10.5194/acp-9-5131-2009, 2009.

Zhao, C. and Wang, Y. H.: Assimilated inversion of NO_x emissions over east Asia using OMI NO_2 column measurements, Geophys. Res. Lett., 36, L06805, doi:10.1029/2008gl037123, 2009.

Zhao, Y., Nielsen, C. P., Lei, Y., McElroy, M. B., and Hao, J.: Quantifying the uncertainties of a bottom-up emission inventory of anthropogenic atmospheric pollutants in China, Atmos. Chem. Phys., 11, 2295–2308, doi:10.5194/acp-11-2295-2011, 2011.

ACPD

11, 29807–29843, 2011

Table 1. Descriptions of VCDs of NO_2 from individual sources derived from model simulations.

Case	Description[a]
1: Ω_m	Simulated by including emissions from all sources
2	Simulated by including all but lightning emissions
3	Simulated by including all but emissions from lightning and fertilizer associated soil sources, i.e., only including anthropogenic, non-fertilizer soil and biomass burning sources
4	Simulated by including emissions from anthropogenic and non-fertilizer soil sources only
5: $\Omega_{m,a}$	Simulated by including anthropogenic emissions only
6: $\Omega_{m,l}$	Case 1–Case 2
7: $\Omega_{m,s}$	(Case 2–Case 3) + (Case 4–Case 5)
8: $\Omega_{m,b}$	Case 3–Case 4

[a] Emissions from all sources are always included for pollutants other than NO_x.

ACPD
11, 29807–29843, 2011

Table 2. Statistics for retrieved and modeled VCDs of NO_2 in January and July 2006.

	Mean	Median	Min	Max	Intercept[c]	Slope[c]	R^{2c}	Intercept[c] Spatially smoothed[d]	Slope[c]	R^{2c}
					January					
Retrieved	5.63	2.54	0.03	62.27						
Modeled	3.62	2.23	0.09	27.62	0.87	0.49	0.64	0.79	0.50	0.70
Predicted[a]	4.89	2.38	0.05	58.12	0.28	0.82	0.83	0.35	0.79	0.88
Sensitivity[b]	5.37	2.87	0.10	45.03	0.53	0.86	0.81	0.42	0.87	0.88
					July					
Retrieved	2.34	1.67	0.06	31.16						
Modeled	1.87	1.47	0.23	10.93	0.61	0.53	0.53	0.47	0.59	0.67
Predicted	2.39	1.65	0.26	31.11	0.16	0.95	0.86	0.06	0.96	0.91
Sensitivity	2.26	1.65	0.31	31.32	0.30	0.84	0.66	0.14	0.89	0.81

[a] Predicted from the regression-based inversion.
[b] Sensitivity simulation using the top-down emissions.
[c] With respect to retrieved VCDs.
[d] After 11 gridboxes by 11 gridboxes horizontal smoothing.

ACPD
11, 29807–29843, 2011

Table 3. Emission budgets over East China (TgN) derived from various inversion calculations.

Case	Description	Anthro. Annual	Lightning	Soil	Anthro. July	Lightning	Soil
	a priori	5.763	0.174	0.324	0.479	0.0507	0.0627
1	Top-down	8.016	0.228	0.424	0.646	0.0623	0.0810
2	Assume seasonality of anthropogenic emissions according to Table 9 of Zhang et al. (2009)	7.830	0.259	0.480	0.640	0.0706	0.0911
3	Assume constant retrieval errors across the seasons	8.306	0.220	0.400	0.668	0.0596	0.0754
4	Use soil emissions from Hudman et al. (2011)	7.876	0.202	0.506	0.6359	0.0537	0.0797
5	Re-allocate group 2 gridboxes to group 1 (and thus skip step 2 in Fig. 6)	8.169	0.201	0.370	0.665	0.0529	0.0693
6	Re-allocate group 2 and 3 gridboxes to group 1 (and thus skip steps 2 and 4 in Fig. 6)	7.720	0.203	0.373	0.642	0.0534	0.0698
7	Use level-2 retrieval data from all 60 pixels	7.789	0.223	0.415	0.633	0.0616	0.0793
8	Keep lightning emissions unchanged	7.950	0.174	0.645	0.644	0.0507	0.1145
9	Keep soil emissions unchanged	8.105	0.238	0.324	0.655	0.0657	0.0627
	Normalized standard deviation of Cases 1–9 relative to Case 1	2.4 %	10.9 %	22.6 %	1.9 %	10.8 %	18.8 %
	A posteriori	7.091	0.217	0.401	0.578	0.0599	0.0769

ACPD
11, 29807–29843, 2011

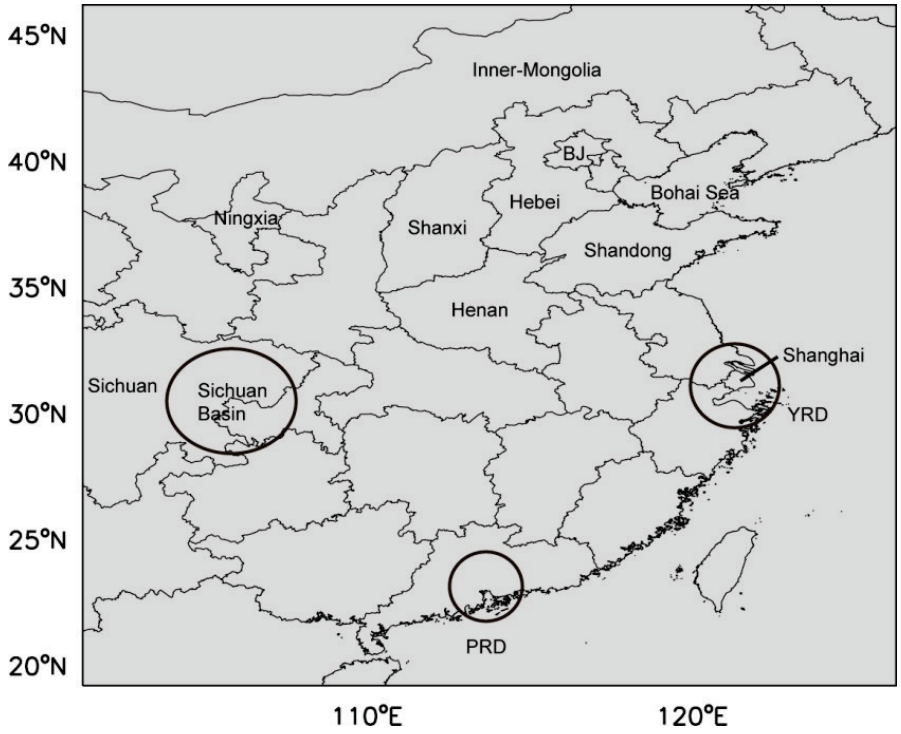

Fig. 1. Regional specifications with provincial boundaries for East China. Also presented are its subregions, provinces and province-level municipalities discussed in the text: the Yangtze River Delta (YRD), the Pearl River Delta (PRD), the Sichuan Basin, the Bohai Sea, Beijing (BJ), Shanghai, Hebei, Henan, Shandong, Shanxi, Ningxia, Inner-Mongolia, and Sichuan.

ACPD
11, 29807–29843, 2011

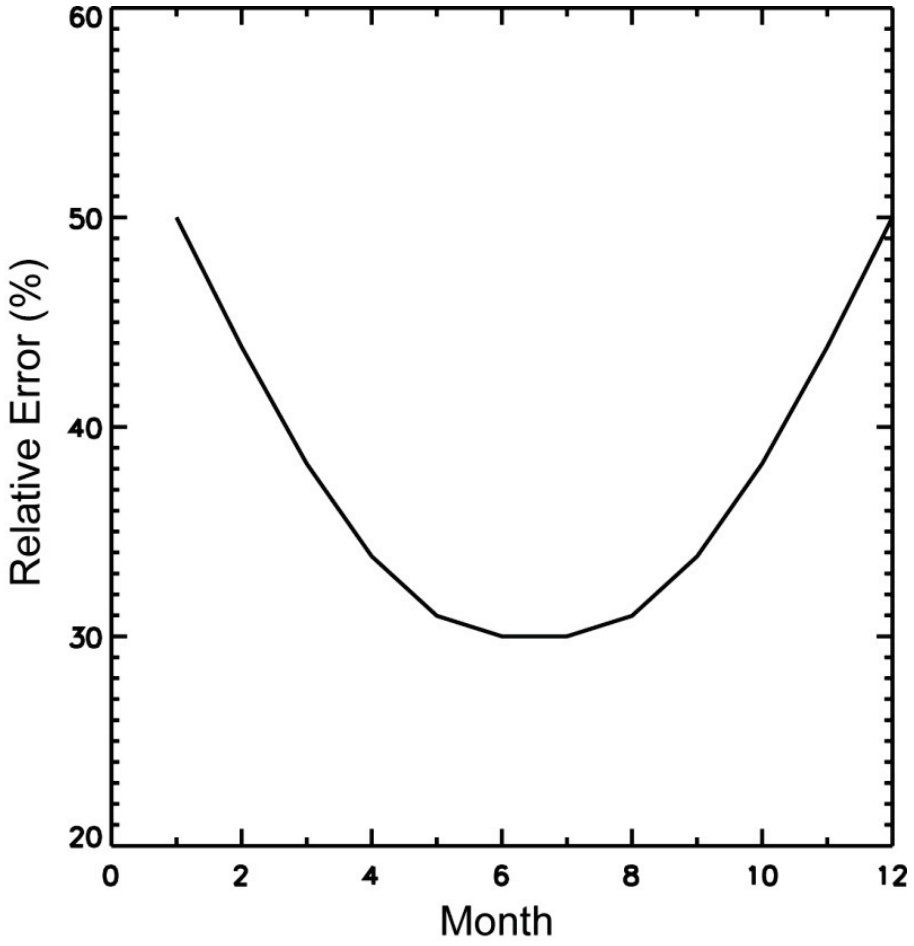

Fig. 2. Relative errors of retrieved VCDs of NO_2 month by month.

ACPD
11, 29807–29843, 2011

Space-based multi-source attribution of NO_x at high resolution

J.-T. Lin

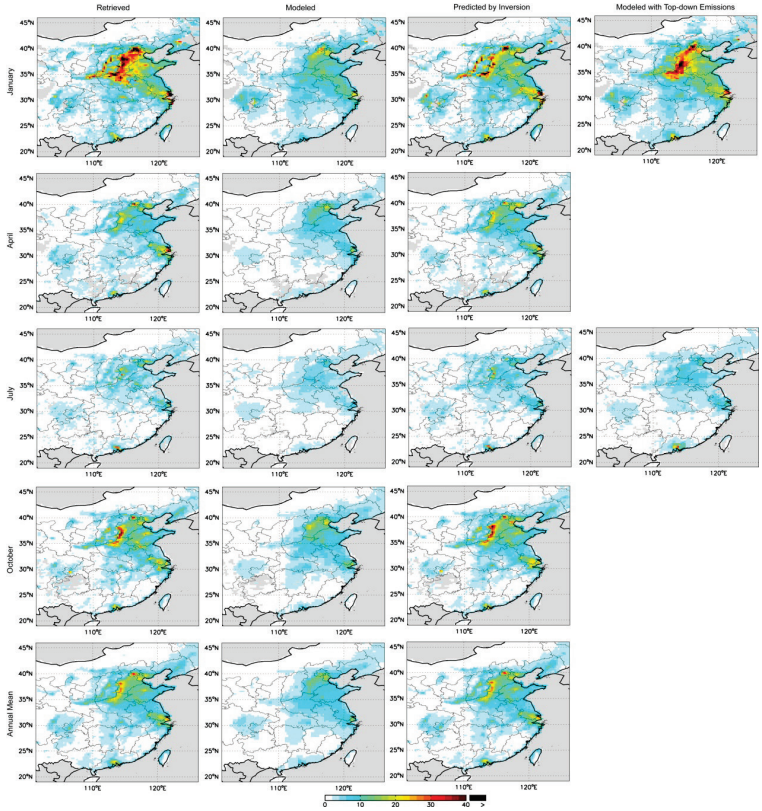

Fig. 3. VCDs of NO_2 (10^{15} molec cm^{-2}) for January, April, July, October and annual average for 2006 retrieved from OMI, simulated by GEOS-Chem with a priori emissions, predicted by the inversion approach, and simulated by GEOS-Chem with top-down emissions. Areas outside the territory of China or without valid retrievals are shown in grey.

ACPD
11, 29807–29843, 2011

Space-based multi-source attribution of NO_x at high resolution

J.-T. Lin

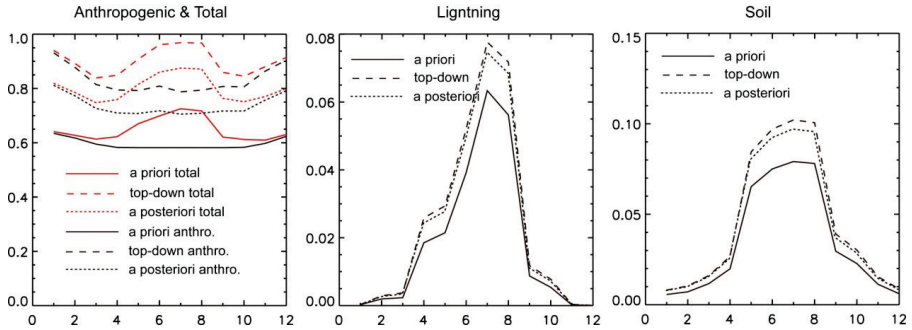

Fig. 4. Seasonal variations of the a priori, top-down and a posteriori anthropogenic, lightning, soil and total emissions of NO_x (10^{15} molec cm^{-2} h^{-1}) over East China for 2006.

ACPD
11, 29807–29843, 2011

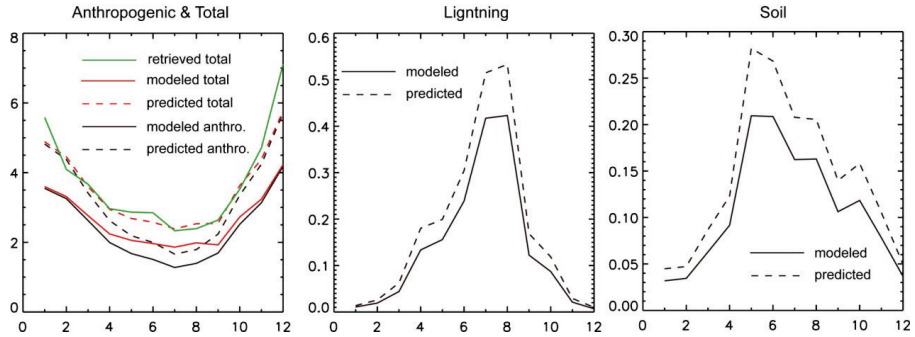

Fig. 5. Seasonal variations of VCDs of NO_2 (10^{15} molec cm^{-2}) over East China for 2006 resulting from anthropogenic, lightning, soil and total emissions of NO_x modeled by GEOS-Chem and predicted by the inversion. Also included is the seasonality of VCDs retrieved from OMI.

ACPD
11, 29807–29843, 2011

Space-based multi-source attribution of NO_x at high resolution

J.-T. Lin

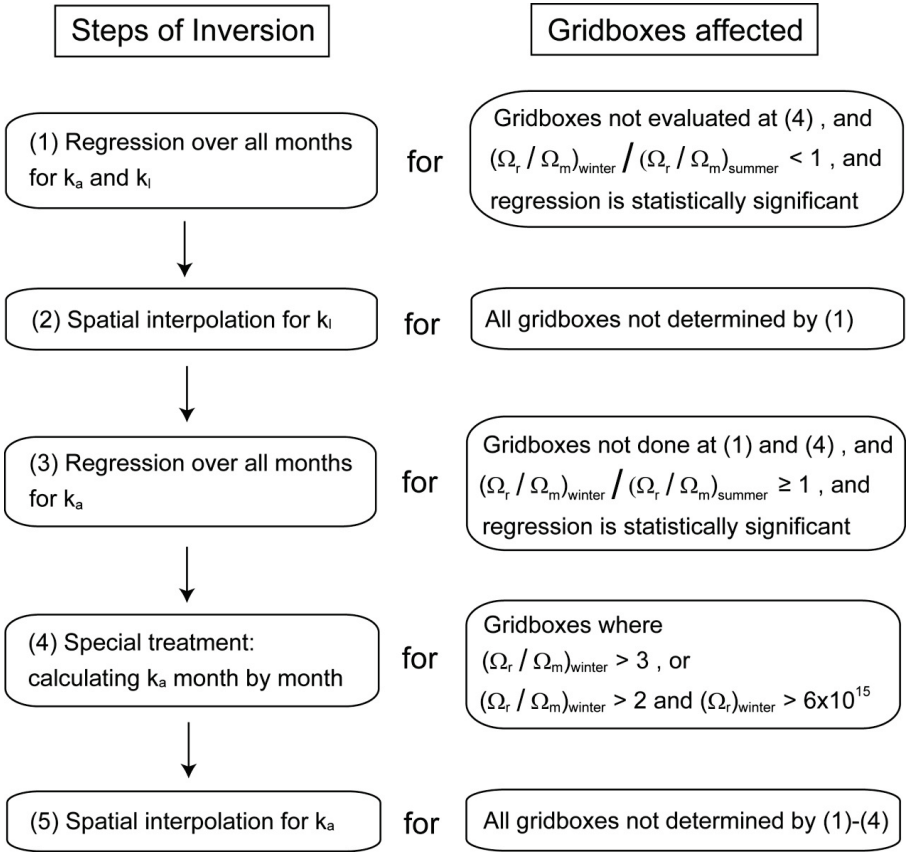

Fig. 6. Description of the regression-based step-by-step inversion process after gridbox grouping. Values of k_l are determined at steps 1 and 2 for all gridboxes and k_a at steps 1, 3, 4, 5. See Sect. 4.1.2 for detailed analysis.

ACPD
11, 29807–29843, 2011

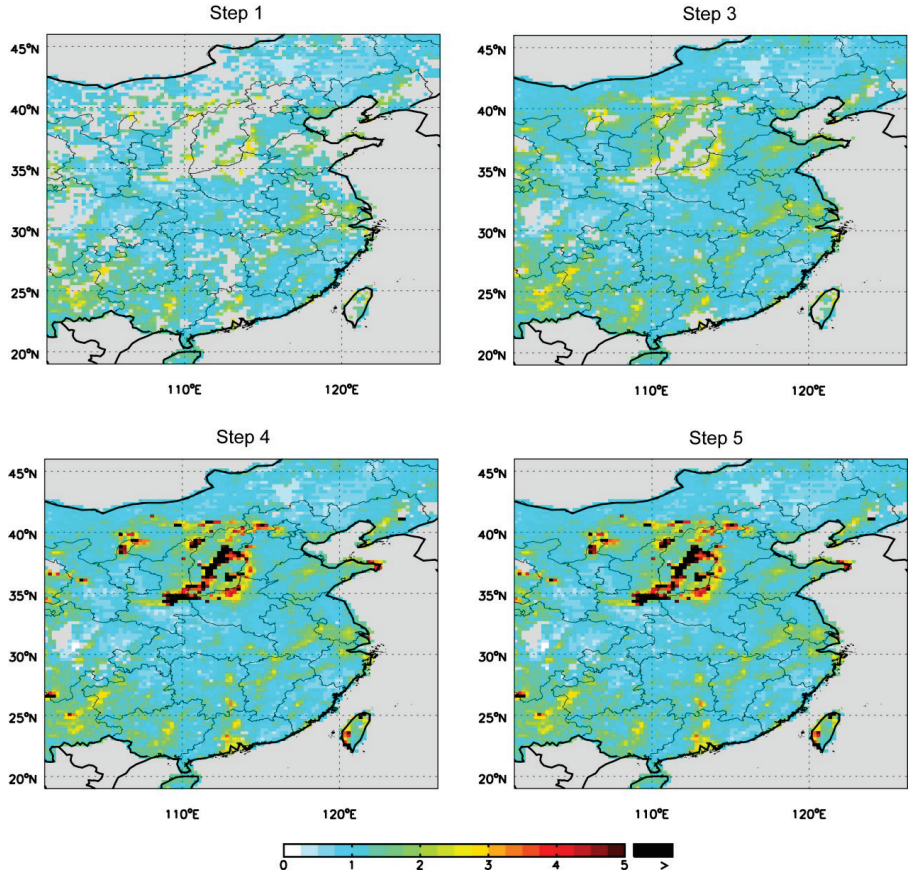

Fig. 7. Scaling factors for anthropogenic emissions (k_a) determined at steps 1, 3, 4 and 5 of the inversion process described in Fig. 6 and Sect. 4.1.2. Step 2 does not affect k_a and thus is not presented. Results at steps 4 and 5 are for January in particular. Areas outside the territory of China or with undetermined k_a are shown in grey.

ACPD
11, 29807–29843, 2011

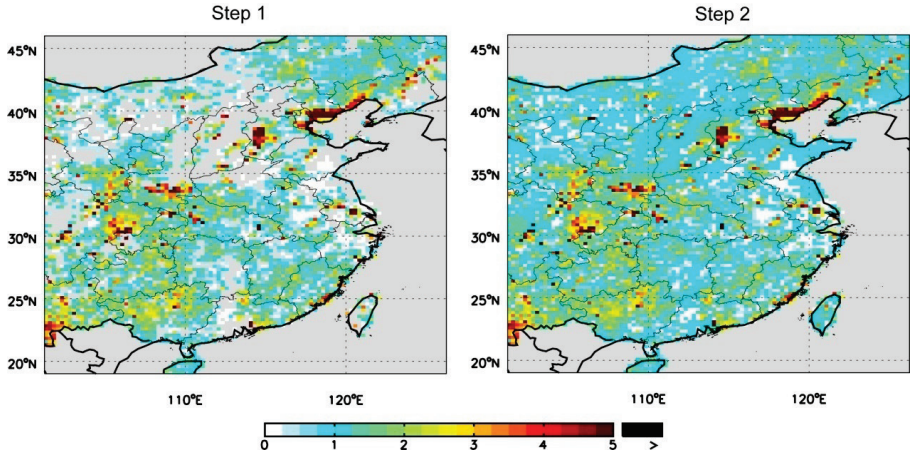

Fig. 8. Scaling factors for lightning/soil emissions (k_l) determined at steps 1 and 2 of the inversion process described in Fig. 6 and Sect. 4.1.2. These two steps decide k_l for all gridboxes. Areas outside the territory of China or with undetermined k_l are shown in grey.

ACPD
11, 29807–29843, 2011

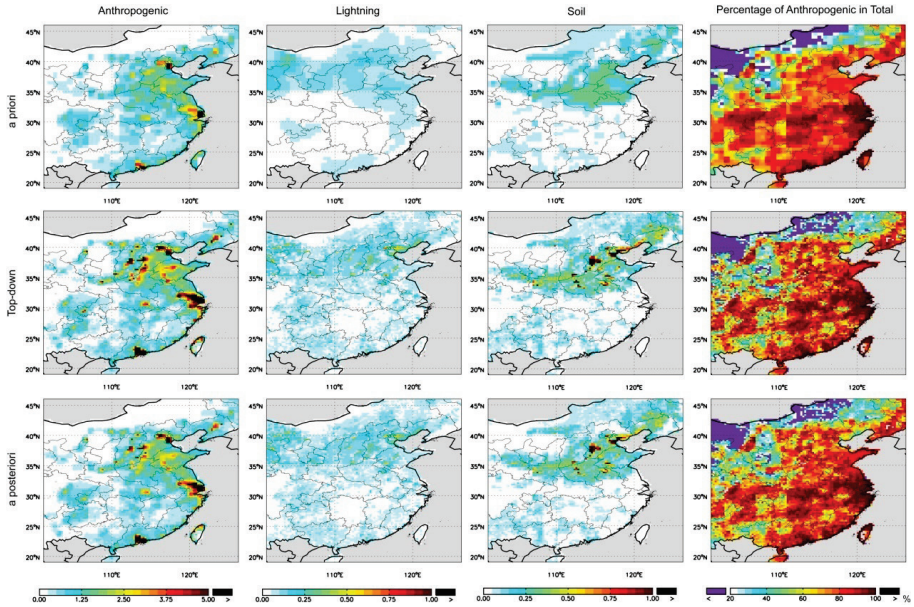

Fig. 9. The a priori, top-down and a posteriori estimates of anthropogenic, lightning and soil emissions of NO_x (10^{15} molec cm^{-2} h^{-1}) and the anthropogenic contributions (in percentage) to total emissions for July 2006 over East China. Areas outside the territory of China are shown in grey.

ACPD
11, 29807–29843, 2011

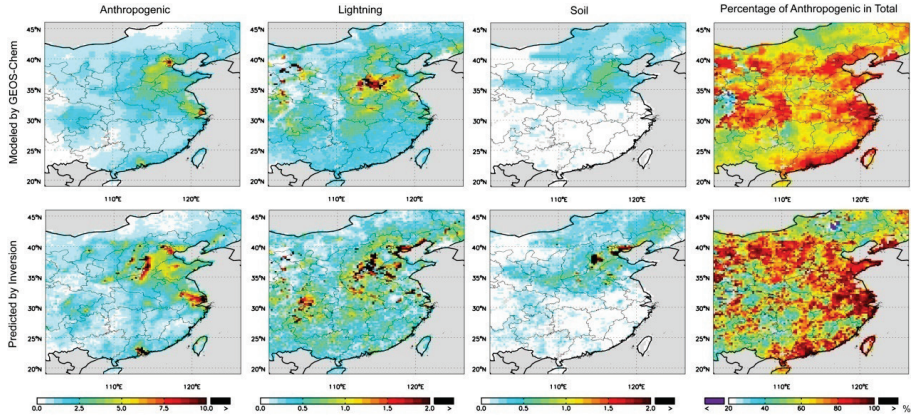

Fig. 10. VCDs of NO_2 (10^{15} molec cm^{-2}) in July 2006 over East China resulting from anthropogenic, lightning and soil emissions of NO_x and the anthropogenic contributions (in percentage) to the total VCDs modeled by GEOS-Chem and predicted by the inversion. Areas outside the territory of China or without valid retrievals are shown in grey.

ACPD
11, 29807–29843, 2011